Radio-frequency Dark Photon Dark Matter across the Sun

Haipeng An,[1,2,*] Fa Peng Huang,[3,4,†] Jia Liu,[5,6,‡] and Wei Xue[7,§]
[1]Department of Physics, Tsinghua University, Beijing 100084, China
[2]Center for High Energy Physics, Tsinghua University, Beijing 100084, China
[3]Department of Physics and McDonnell Center for the Space Sciences, Washington University, St. Louis, Missouri 63130, USA
[4]TianQin Research Center for Gravitational Physics and School of Physics and Astronomy, Sun Yat-sen University (Zhuhai Campus), Zhuhai 519082, China
[5]School of Physics and State Key Laboratory of Nuclear Physics and Technology, Peking University, Beijing 100871, China
[6]Center for High Energy Physics, Peking University, Beijing 100871, China
[7]Department of Physics, University of Florida, Gainesville, Florida 32611, USA

(Received 9 November 2020; revised 1 March 2021; accepted 7 April 2021; published 5 May 2021)

The Dark photon as an ultralight dark matter candidate can interact with the standard model particles via kinetic mixing. We propose to search for the ultralight dark photon dark matter using radio telescopes with solar observations. The dark photon dark matter can efficiently convert into photons in the outermost region of the solar atmosphere, the solar corona, where the plasma mass of photons is close to the dark photon rest mass. Because of the strong resonant conversion and benefiting from the short distance between the Sun and the Earth, the radio telescopes can lead the dark photon search sensitivity in the mass range of 4×10^{-8}–4×10^{-6} eV, corresponding to the frequency 10–1000 MHz. As a promising example, the low-frequency array telescope can reach the kinetic mixing $\epsilon \sim 10^{-13}$ (10^{-14}) within 1 (100) h of solar observations. The future experiment square kilometer array phase 1 can reach $\epsilon \sim 10^{-16}$–10^{-14} with 1 h of solar observations.

DOI: 10.1103/PhysRevLett.126.181102

Introduction.—The ultralight bosonic fields are attractive dark matter (DM) candidates. Within them, the QCD axions, axionlike particles, and dark photons are well-studied scenarios [1,2]. Kinetic mixing dark photon is one of the simplest extensions of new physics beyond the standard model (SM) via a marginal operator, which is well motivated at low energies. It can also constitute DM [3–7] and may reveal the theories beyond the SM [8–12]. There are many searches looking for dark photon or dark photon DM. For mass $\lesssim 10^{-9}$ eV, the dark photon DM can be constrained by the observation of astronomical radio sources [13], cosmic microwave background (CMB) spectrum distortion, Big Bang nucleosynthesis, Lyman-α, and heating of primordial plasma [6,14–21]. In the optical mass range of 0.1–10 eV, dark photon DM can be detected by the optical haloscope [22]. For dark photon DM with a mass larger than about $\mathcal{O}(10)$ eV, it can be absorbed in the underground DM detectors and produce electronic recoil signals [23–26]. Dark photon lighter than the temperatures at the center of stars can also be produced inside stars and suffer stellar cooling constraints [27–30]. Dark photons produced inside the Sun can be detected by DM direct detection experiments [30–32].

In this Letter, we focus on the radio mass window (10^{-8}–10^{-6} eV) for dark photon and assume it constitutes all the DM. This mass window is of particular interest because it overlaps with the regions that dark photon DM is naturally produced by mechanisms, including the inflationary fluctuations [7,33], parametric resonances [34–37], cosmic strings [38], the misalignment with nonminimal coupling to the gravity [6,39] (see the ghost instability discussion in [40]), and production by inflaton motion [41]. The relevant searches for dark photon DM are haloscope experiments [42–47], dish antenna experiments [48,49], plasma telescopes [50], and CMB spectrum distortion [6,19]. The searches include direct detection of local dark photon DM in laboratories and observation on its impact in the early Universe. Differently, we proposal to look for resonant conversion of dark photon DM $A' \to \gamma$ at the Sun through the radio telescopes for solar observations. This is an indirect detection of dark photon DM signal from the closest astronomical object, the Sun. It provides competitive sensitivities even with existing radio telescopes and opens vast new parameter space with future setups.

Below the electroweak scale, the minimal coupling between the dark photon and the standard model particles can be described by the following Lagrangian density:

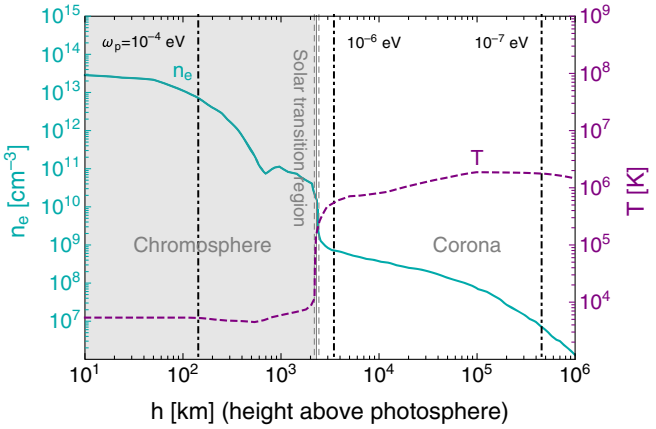

FIG. 1. The electron number density (green solid line) and the temperature (purple dashed line) distribution for the quiet Sun from [53]. In the gray shaded region, the converted photons produced below the solar transition region cannot propagate out of the Sun. The radius for photon plasma mass $\omega_p = 10^{-4}, 10^{-6}, 10^{-7}$ eV are shown in vertical dot-dashed lines. The height above the photosphere h and the radius r has the relation $r \equiv h + r_{\rm ps}$, where $r_{\rm ps} = 695510$ km is the radius for the solar photosphere.

$$\mathcal{L} = -\frac{1}{4}F'_{\mu\nu}F'^{\mu\nu} + \frac{1}{2}m_{A'}^2 A'_\mu A'^\mu - \frac{1}{2}\epsilon F_{\mu\nu}F'^{\mu\nu}, \quad (1)$$

where $F_{\mu\nu}$ is the photon field strength, A' is the dark photon field, $F'^{\mu\nu}$ is the dark photon field strength, and ϵ is the kinetic mixing. With this mixing term, the dark photons can oscillate resonantly into photons in thermal plasma once the plasma frequency $\omega_p \approx m_{A'}$. The plasma frequency for nonrelativistic plasma relies on the electron density n_e,

$$\omega_p = \left(\frac{4\pi\alpha n_e}{m_e}\right)^{1/2} = \left(\frac{n_e}{7.3\times 10^8\ \text{cm}^{-3}}\right)^{1/2} \mu\text{eV}, \quad (2)$$

where α and m_e are the fine structure constant and electron mass, respectively. In the Sun's corona, $n_e \sim 10^6$–10^{10} cm^{-3} is shown in Fig. 1. Hence the range of the plasma frequency ω_p is from 4×10^{-8} to 4×10^{-6} eV. If $m_{A'}$ falls in this range, A' can resonantly convert into a monochromatic radio wave in the corona, with the peak frequency corresponding to $m_{A'}$, which is in the range of about 10–1000 MHz. This frequency range happens to be in the sensitive region of the terrestrial radio telescopes, such as the low-frequency array (LOFAR) [51] and square kilometer array (SKA) [52]. Therefore, we propose to use radio telescopes to search for dark photon DM in this mass range.

Resonant conversion in the Sun's corona.—The average conversion probability of a dark photon particle flying across the Sun's corona is the time integral of the decay rate of $A' \to \gamma$, written as

$$P_{A'\to\gamma}(v_r) = \int \frac{dt}{2\omega}\frac{d^3p}{(2\pi)^3 2\omega}(2\pi)^4\delta^4(p^\mu_{A'} - p^\mu_\gamma)\frac{1}{3}\sum_{\rm pol}|\mathcal{M}|^2$$
$$= \frac{2}{3}\times\pi\epsilon^2 m_{A'} v_r^{-1}\left|\frac{\partial \ln\omega_p^2(r)}{\partial r}\right|^{-1}_{\omega_p(r)=m_{A'}}. \quad (3)$$

Here we take average of the initial state of A'. During the structure formation, the momentum direction of A' is randomly rotated in the gravitational potential. Therefore, each mode (either transverse or longitudinal) has the equal probability, 1/3. Since only the transverse modes of photons can survive outside the plasma and propagate to the Earth, we only sum over the transverse polarizations in the final state. In the second line, v_r is the velocity projected on the radial direction of the Sun. Because of the spherical distribution of n_e, ω_p only changes in the radial direction.

Equation (3) utilized the quantum field method to calculate the $1\to1$ conversion and the matrix element $\mathcal{M}$ is derived by directly using the kinetic mixing operator $\frac{1}{2}\epsilon F_{\mu\nu}' F^{\mu\nu}$. Because of the momentum conservation, it only applies for the resonant conversion $\omega_p = m_{A'}$. An equivalent way to calculate the conversion rate is to solve the linearized wave equations for the photon and dark photon [54], which works for both resonant and nonresonant conversion. After applying the saddle point approximation, the result is the same as in Eq. (3). It can be explicitly shown that the nonresonant contribution is negligible. The detailed calculations for the two methods are given in the Supplemental Material [55]. Finally, the above result is in agreement with the probability for inverse conversion $\gamma \to A'$ [14].

Given the conversion probability, the radiation power $\mathcal{P}$ per solid angle $d\Omega$ at the conversion radius r_c is

$$\frac{d\mathcal{P}}{d\Omega} \approx 2\times\frac{1}{4\pi}\rho_{\rm DM} v_0 \int_0^b dz 2\pi z P_{A'\to\gamma}(v_r)$$
$$= P_{A'\to\gamma}(v_0)\rho_{\rm DM} v(r_c) r_c^2, \quad (4)$$

where we consider DM density $\rho_{\rm DM} = 0.4$ GeV cm^{-3} completely composed of dark photon. Its average velocity $v_0 \simeq 220$ km/s and the resonant conversion happens at the solar radius r_c. The parameter z is the impact parameter at infinity for the incoming A', while b is the largest value of the impact parameter such that A' can reach the conversion shell at $r = r_c$. Because of the gravitational focusing enhancement, $b = r_c v(r_c)/v_0$ will be larger than r_c, in general, by a factor of about 2–3 in numeric calculations. The velocity of A' at radius r_c is given by $v(r_c) = \sqrt{v_0^2 + 2G_N M_\odot/r_c}$, with G_N being the gravitational constant and $M_\odot$ the solar mass. The radial direction velocity at the conversion point is $v_r(z) = \sqrt{2G_N M_\odot/r_c + v_0^2 - v_0^2 z^2/r_c^2}$. The factor 2 in Eq. (4) counts the DM coming in and going out of the resonant layer. The converted photon from DM coming in

will be reflected, because when the photon frequency is smaller than the plasma mass, the total reflection will happen.

The spectral power flux density emitted per unit solid angle is given as

$$S_{\rm sig} = \frac{1}{d^2}\frac{1}{\mathcal{B}}\frac{d\mathcal{P}}{d\Omega}, \tag{5}$$

where $d = 1$ A.U. is the distance from the Earth to the Sun, $\mathcal{B}$ is the optimized bandwidth, which is set as the larger one of the signal bandwidth $B_{\rm sig}$ and the telescope spectral resolution $B_{\rm res}$, namely, $\mathcal{B} = \max(B_{\rm sig}, B_{\rm res})$. The signal bandwidth $B_{\rm sig}$ is due to the dispersion of the dark photons,

$$B_{\rm sig} \approx \frac{m_{A'} v_0^2}{2\pi} \sim 130\ {\rm Hz} \times \frac{m_{A'}}{\mu{\rm eV}}, \tag{6}$$

which is normally smaller than $B_{\rm res}$, and the telescope spectral resolution $B_{\rm res}$ depends on the property of the telescope.

The photon propagation.—After the conversion, the propagation of the radio waves in the thermal plasma follows the refraction law, $n \sin\theta = {\rm const}$, where n is the refractive index and θ is the incident angle. In nonrelativistic plasma, n can be expressed as

$$n(\omega) = (1 - \omega_p^2/\omega^2)^{1/2}, \tag{7}$$

where $n(\omega)$ equals the group velocity of the radio waves, i.e., the photon speed. In the resonant region, the dark photon DM has a velocity of about $v \sim 10^{-3}$–10^{-2}. As a result, the refractive index at the resonant region is in the range of $n_{\rm res} \sim 10^{-3}$–10^{-2}, which is much smaller than 1. From Fig. 1, the electron density n_e decreases quickly with the increase of r. Consequently, once the photon leaves the resonant region, the refractive index will quickly go back to 1, $n_{\rm out} \sim 1$. Thus, according to the refractive law, the incident angle outside the resonant region can be written as

$$\sin\theta_{\rm out} = \frac{n_{\rm res}}{n_{\rm out}} \times \sin\theta_{\rm res} \lesssim 10^{-3}\text{–}10^{-2}. \tag{8}$$

Therefore, the direction of the converted photon is approximately along the gradient of the electron density $-\nabla n_e$. Considering the conversion happened when the dark photon flies into the Sun and the converted photon moves into the denser region, we expect that electromagnetic waves are always total reflected away from the region where $\omega < \omega_p$. Hence the above discussion of the final photon direction applies after the total reflection. If the electron distribution in the Sun's corona is spherical, the converted radio waves will all propagate along with the radial direction of the Sun. In this case, all the converted radio waves observed on the Earth's surface are from the center of the solar plate. However, there are turbulences and flares in the Sun's corona, which makes n_e nonspherical and even evolve with time. It will affect the gradient direction of n_e, thus modify the outgoing direction of the photon. However, such modification should not have preferred directions, unless there are underlying substructures. Therefore, we ignore those modifications and assume that, on average, the outgoing converted photons are isotropic.

Once converted, the radio waves can be absorbed or scattered in the plasma, which is characterized by opacity. It turns out that the dominant absorption process is the inverse bremsstrahlung process. In the corona sphere, the temperature is as high as 10^6 K, which is much larger than the ionization energy of the hydrogen atom. As a result, the Born approximation can be used to calculate the absorption rate. Since we are interested in the radio wave frequency, it satisfies $\omega \ll T \ll m_e$. The absorption rate of the inverse bremsstrahlung process can be calculated as

$$\Gamma_{\rm inv} \approx \frac{8\pi n_e n_N \alpha^3}{3\omega^3 m_e^2}\left(\frac{2\pi m_e}{T}\right)^{1/2} \log\left(\frac{2T^2}{\omega_p^2}\right)(1 - e^{-\omega/T}), \tag{9}$$

where the singularity at $\omega = 0$ clearly shows the effect of the infrared enhancement. n_N is the number density of charged ions. The logarithmic factor is from the long-range effect of the Coulomb interaction, which is cut off by the Debye screening effect. The factor $(1 - e^{-\omega/T})$ is due to the stimulated radiation. The above calculation is in good agreement with Ref. [56], except for a minor difference in the argument of the logarithmic factor.

Besides the inverse bremsstrahlung process, there is also a contribution from the Compton scattering with the rate given as

$$\Gamma_{\rm Com} = \frac{8\pi\alpha^2}{3m_e^2} n_e. \tag{10}$$

The Compton scattering can shift the photon energy by a few percent due to the velocity of the electrons. This change is normally larger than the optimized bandwidth. As a conservative consideration, we add up the two contributions and have the attenuation rate $\Gamma_{\rm att} = \Gamma_{\rm inv} + \Gamma_{\rm Com}$ for the converted photon. Numerically, the inverse bremsstrahlung dominates. The survival probability P_s for the converted photons to escape the Sun is to add the two rates,

$$P_s \equiv e^{-\int \Gamma_{\rm att} dt} \simeq \exp\left(-\int_{r_c}^{r_{\rm max}} \Gamma_{\rm att} dr/v_r\right), \tag{11}$$

which represents the chance of the photons being not scattered or absorbed during the propagation. We terminate the integration at $r_{\rm max} = 10^6$ km $+ r_{\rm ps}$ due to the available electron density data [53], where $r_{\rm ps} = 695510$ km is the photosphere radius. Further extending the range will not change the result significantly, because the electron density is too low, such that the interaction rate is negligible.

Dark photon DM with mass $> 4 \times 10^{-6}$ eV can also convert resonantly to photons in the Sun's chromosphere. However, the temperature of the chromosphere is only about 10^3 K, which is about 3 orders of magnitude smaller than the temperature of the corona. This makes the inverse bremsstrahlung absorption much stronger in the chromosphere than in the corona. Furthermore, the electron number density, as shown in Fig. 1, is also orders of magnitude larger, and so is the density of charged ions. Therefore, the radio waves produced in the chromosphere cannot propagate out.

In summary, the dark photon DM's resonant conversion happening in the Sun's corona can propagate to the Earth's surface. In terms of distance, the region 2300 km above the photosphere (higher than the solar transition region) is our signal region. This corresponds to the unshaded region in Fig. 1. The relevant observed photon frequency is $\lesssim$1000 MHz and dark photon mass is $m_{A'} \lesssim 4 \times 10^{-6}$ eV. In the above discussions, we only use the well-accepted electron density and temperature profiles as shown in Fig. 1. They are good approximations and have acceptable uncertainties for the signal calculation. More discussions on the solar models and the corresponding uncertainties are given in the Supplemental Material [55] (which includes Refs. [57–63]).

The sensitivity of radio telescopes.—The minimum detectable flux density of a radio telescope is [64]

$$S_{\rm min} = \frac{\rm SEFD}{\eta_s \sqrt{n_{\rm pol} \mathcal{B} t_{\rm obs}}}, \tag{12}$$

where $n_{\rm pol} = 2$ is the number of polarization, $t_{\rm obs}$ is the observation time, and η_s is the system efficiency. In our analysis, we take $\eta_s = 0.9$ for SKA [64], and $\eta_s = 1$ for LOFAR [65]. The values of the telescope spectral resolution $B_{\rm res}$ for LOFAR and SKA are listed in Table I, which are much larger than the signal bandwidth $B_{\rm sig}$ given in Eq. (6). Therefore, in our calculation, we always have $\mathcal{B} \simeq B_{\rm res}$. In Eq. (12), SEFD is the system equivalent flux density, defined as

$$\rm SEFD = 2 k_B \frac{T_{\rm sys} + T_\odot^{\rm nos}}{A_{\rm eff}}, \tag{13}$$

TABLE I. The frequency range, telescope spectral resolution $B_{\rm res}$, averaged system temperature $T_{\rm sys}$, and averaged effective area $A_{\rm eff}$ in the different frequency bands for SKA1 and LOFAR.

Name	f (MHz)	$B_{\rm res}$ (kHz)	$\langle T_{\rm sys} \rangle$ (K)	$\langle A_{\rm eff} \rangle$ (m^2)
SKA1-low	(50, 350)	1	680	2.2×10^5
SKA1-mid $B1$	(350, 1050)	3.9	28	2.7×10^4
SKA1-mid $B2$	(950, 1760)	3.9	20	3.5×10^4
LOFAR	(10, 80)	195	28 110	1830
LOFAR	(120, 240)	195	1 770	1530

where k_B is the Boltzmann constant, $T_{\rm sys}$ is the antenna system temperature, $A_{\rm eff}$ is the antenna effective area of the array, and $T_\odot^{\rm nos}$ is the antenna noise temperature increase when pointing to the Sun.

We propose to use the radio telescope arrays SKA and LOFAR to search for the radio waves converted from dark photon DM at the Sun's corona. We consider SKA phase 1 (SKA1) as the benchmark of a future telescope to study the reach of dark photon DM. It has a low-frequency aperture array (SKA1-low) and a middle-frequency aperture array (SKA1-mid) [64]. SKA1-low covers the (50,350) MHz frequency band. SKA1-mid covers six frequency bands with frequency ranges (350,1050), (950,1760), (1650,3050), (2800,5180), (4600,8500), and (8300,15300) MHz. In this analysis, to partially cover the frequency range of the converted radio wave, we use the SKA-low and the first two frequency bands of SKA-mid, denoted as mid $B1$ and mid $B2$, respectively. LOFAR, as an existing radio telescope, can be used for dark photon hunting as well. Indeed, one of the key science projects for LOFAR is to study solar physics. In its radio spectrometer mode, the intensity of the solar radio radiation over time is recorded. LOFAR covers the frequency ranges of (10,80) and (120,240) MHz.

To calculate the minimum detectable flux $S_{\rm min}$ given in Eq. (12), we need to determine the corresponding detector parameters, such as the telescope spectral resolution $B_{\rm res}$, the system temperature $T_{\rm sys}$, the solar noise temperature $T_\odot^{\rm nos}$, and the effective area $A_{\rm eff}$. Table I lists the average values of these parameters for each telescope, and the details to achieve these parameters are given as follows:

Spectral resolution $B_{\rm res}$: Because of 2.5×10^5 fine frequency channels in SKA1-low, its channel bandwidth can reach $B_{\rm res} = 1$ kHz, while the bandwidth for SKA1-mid $B1$ and SKA1-mid $B2$ are set to $B_{\rm res} = 3.9$ kHz [64]. For LOFAR, The spectral resolution $B_{\rm res}$ is taken as 195 kHz [51,66].

System temperature $T_{\rm sys}$ and effective area $A_{\rm eff}$: The system temperature for SKA1-low can be approximated as $T_{\rm sys}^{\rm low} \approx T_{\rm rec} + T_{\rm sky}$, where the sky noise $T_{\rm sky} \approx 1.23 \times 10^8$ K$(\rm MHz/\mathit{f})^{2.55}$ and the receiver noise $T_{\rm rec} = 40$ K $+ 0.1 T_{\rm sky}$ [64]. For SKA1-mid, the average system temperatures for bands 1–5 are 28, 20, 20, 22, and 25 K, respectively [64]. The effective area $A_{\rm eff}$ is derived using the system sensitivity $A_{\rm eff}/T_{\rm sys}$ in [51]. The parameters of LOFAR like $A_{\rm eff}$ can be directly found in [51], while $T_{\rm sys}$ can be inferred from SEFD. Note that, in the numeric calculation, the parameters $A_{\rm eff}$ and $T_{\rm sys}$ depend on the frequency.

Solar noise temperature $T_\odot^{\rm nos}$: $T_\odot^{\rm nos}$ can be calculated under the blackbody assumption for a quiet Sun [67,68]. The ratio of $T_\odot^{\rm nos}$ and the brightness temperature of the quiet Sun T_b, $T_\odot^{\rm nos}/T_b$, has been given for different half-power beamwidth (HPBW or -3 dB beam width) and beam pointing offset. It is easy to understand that the ratio should always be smaller than 1, because the noise temperature cannot be higher than the source itself. The result shows

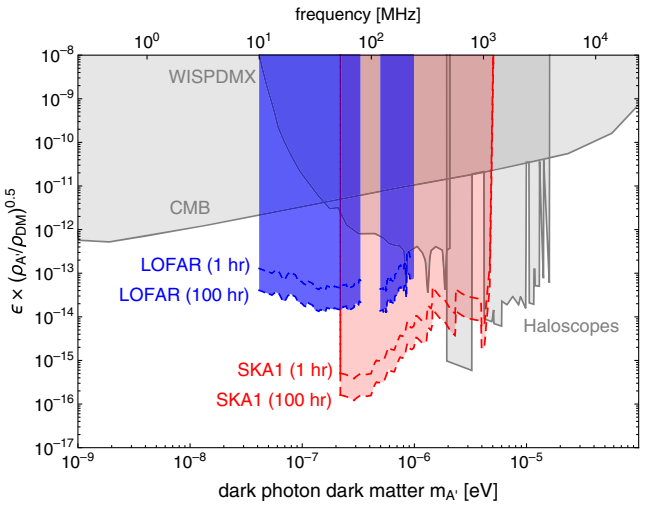

FIG. 2. The sensitivity reach of dark photon dark matter for LOFAR (blue) and SKA1 (red) telescopes with 1 or 100 hours solar observations. The constraints are obtained from the existing haloscope axion searches [6,42–46], recent WISPDMX dark photon searches [47] and the CMB distortion [6,19]. For both signal and existing constraints, $\rho_{\rm DM} = \rho_{A'}$ is assumed.

that, for the antenna with HPBW smaller than the angular diameter of the Sun disk, this ratio is close to 1 when beam is on the solar disk. The HPBW for the SKA1-low current design is about 4 arc min at the baseline frequency 110 MHz [69], while the angular diameter of the Sun is as large as 31.8 arc min. Therefore, SKA1-low can be considered as a high-gain antenna with a very narrow beam. The SKA1-mid has even smaller HPBW than SKA1-low; thus throughout the calculation, we take $T_\odot^{\rm nos} = T_b$. The spectral brightness temperature $T_b(f)$ is calculated using the quiet Sun flux density from [68,70]. Regarding the LOFAR beamwidth, the HPBW of LOFAR ranges from (1.3,19) degrees [51]. Therefore, it is much larger than the angular diameter of the Sun. Following the procedure of [68], we use the antenna diameters of LOFAR to calculate the ratio $T_\odot^{\rm nos}/T_b$ for the Sun as a function of frequency. This ratio is far smaller than 1 because much of the photon flux goes outside the HPBW. It is important to remark that this ratio should also work for the signals because both background and signal emissions are originated from the Sun. We find that, for the frequency smaller than 55 MHz, the system temperature $T_{\rm sys}$ dominates over the solar contribution $T_\odot^{\rm nos}$.

Results and discussions.—Requiring $S_{\rm sig} \times P_s = S_{\rm min}$, one can obtain the sensitivities on the kinetic mixing ϵ from radio telescopes. The sensitivity reaches of dark photon DM for SKA and LOFAR are given in Fig. 2, where both the signal and constraints are plotted under the assumption $\rho_{\rm DM} = \rho_{A'}$. The blue regions show the physics potential of LOFAR with 1 and 100 h observation time, which is 1–2 orders of magnitude better than the existing limits from haloscope limits [6,42–46], recent WISPDMX constraint [47], and the CMB distortion [6,19]. SKA1 has smaller $T_{\rm sys}$, larger $A_{\rm eff}$, and better spectral resolution $B_{\rm res}$. Its sensitivities with 1 and 100 h observation time are shown in the red shaded region. With the same operation time, it can improve the reach of ϵ by another 1–2 orders of magnitude compared with LOFAR.

In conclusion, we propose to search for the radio frequency dark photon DM from 10–1000 MHz, with radio telescopes. In this frequency regime, we show that the dark photon DM can convert resonantly into monochromatic radio waves in the solar corona. In this mass window, the existing LOFAR telescope can achieve a sensitivity of $\sim 10^{-13} - 10^{-14}$ on the kinetic mixing ϵ, and the planned SKA1 can achieve a sensitivity of $\sim 10^{-14}$–10^{-16}. Despite SKA and LOFAR, other radio telescopes that may be used in the dark photon DM search are the Murchison widefield array [71], Arecibo [72], the Karl G. Jansky very large array [73], and the five-hundred-meter aperture spherical radio telescope [74]. In the future, the SKA phase 2 [52] can further improve the SEFD sensitivity to sub-μJy and explore more parameter space of the dark photon DM.

The authors would like to thank Goerge Heald, Judith Irwin, Ben Safdi, Lijing Shao, David Tanner, Aaron Vincent, and Yiming Zhong for helpful discussions. The authors would like to express a special thanks to the Mainz Institute for Theoretical Physics (MITP) of the Cluster of Excellence PRISMA+ (Project ID 39083149) workshop for their hospitality and support. H. A. and W. X. thank the Erwin Schrödinger International Institute for hospitality during the completion of this work. The work of H. A. is supported by NSFC under Grant No. 11975134, the National Key Research and Development Program of China under Grant No. 2017YFA0402204, and the Tsinghua University Initiative Scientific Research Program. F. P. H. is supported by the McDonnell Center for the Space Sciences. The work of J. L. is supported by NSFC under Grant No. 12075005 and by Peking University under startup Grant No. 7101502458. The work of W. X. is supported by the DOE Award No. DE-SC0010296.

*anhp@mail.tsinghua.edu.cn
†fapeng.huang@wustl.edu
‡Corresponding author.
jialiu@pku.edu.cn
§weixue@ufl.edu

[1] R. Essig *et al.*, Working group report: New light weakly coupled particles, in *Proceedings of the 2013 Community Summer Study on the Future of U.S. Particle Physics, Snowmass on the Mississippi (CSS2013), Minneapolis, MN, USA 2013*, http://www.slac.stanford.edu/econf/C1307292/docs/IntensityFrontier/NewLight-17.pdf.

[2] M. Battaglieri *et al.*, U.S. cosmic visions: New ideas in dark matter 2017: Community report, in U.S. Cosmic Visions: New Ideas in Dark Matter, College Park, MD, USA, 2017,

http://lss.fnal.gov/archive/2017/conf/fermilab-conf-17-282-ae-ppd-t.pdf.
[3] B. Holdom, Two U(1)'s and epsilon charge shifts, Phys. Lett. **166B**, 196 (1986).
[4] J. Redondo and M. Postma, Massive hidden photons as lukewarm dark matter, J. Cosmol Astropart. Phys. 02 (**2009**) 005.
[5] A. E. Nelson and J. Scholtz, Dark light, dark matter and the misalignment mechanism, Phys. Rev. D **84**, 103501 (2011).
[6] P. Arias, D. Cadamuro, M. Goodsell, J. Jaeckel, J. Redondo, and A. Ringwald, WISPy cold dark matter, J. Cosmol. Astropart. Phys. 06 (2012) 013.
[7] P. W. Graham, J. Mardon, and S. Rajendran, Vector dark matter from inflationary fluctuations, Phys. Rev. D **93**, 103520 (2016).
[8] K. R. Dienes, C. F. Kolda, and J. March-Russell, Kinetic mixing and the supersymmetric gauge hierarchy, Nucl. Phys. **B492**, 104 (1997).
[9] S. A. Abel and B. W. Schofield, Brane anti-brane kinetic mixing, millicharged particles and SUSY breaking, Nucl. Phys. **B685**, 150 (2004).
[10] S. A. Abel, J. Jaeckel, V. V. Khoze, and A. Ringwald, Illuminating the hidden sector of string theory by shining light through a magnetic field, Phys. Lett. B **666**, 66 (2008).
[11] S. A. Abel, M. D. Goodsell, J. Jaeckel, V. V. Khoze, and A. Ringwald, Kinetic mixing of the photon with hidden U(1)s in string phenomenology, J. High Energy Phys. 07 (2008) 124.
[12] M. Goodsell, J. Jaeckel, J. Redondo, and A. Ringwald, Naturally light hidden photons in LARGE volume string compactifications, J. High Energy Phys. 11 (2009) 027.
[13] A. P. Lobanov, H. S. Zechlin, and D. Horns, Astrophysical searches for a hidden-photon signal in the radio regime, Phys. Rev. D **87**, 065004 (2013).
[14] A. Mirizzi, J. Redondo, and G. Sigl, Microwave background constraints on mixing of photons with hidden photons, J. Cosmol. Astropart. Phys. 03 (2009) 026.
[15] K. E. Kunze and M. A. Vázquez-Mozo, Constraints on hidden photons from current and future observations of CMB spectral distortions, J. Cosmol. Astropart. Phys. 12 (2015) 028.
[16] S. Dubovsky and G. Hernández-Chifflet, Heating up the galaxy with hidden photons, J. Cosmol. Astropart. Phys. 12 (2015) 054.
[17] E. D. Kovetz, I. Cholis, and D. E. Kaplan, Bounds on ultralight hidden-photon dark matter from observation of the 21 cm signal at cosmic dawn, Phys. Rev. D **99**, 123511 (2019).
[18] M. Pospelov, J. Pradler, J. T. Ruderman, and A. Urbano, Room for New Physics in the Rayleigh-Jeans Tail of the Cosmic Microwave Background, Phys. Rev. Lett. **121**, 031103 (2018).
[19] S. D. McDermott and S. J. Witte, Cosmological evolution of light dark photon dark matter, Phys. Rev. D **101**, 063030 (2020).
[20] A. Caputo, H. Liu, S. Mishra-Sharma, and J. T. Ruderman, Dark Photon Oscillations in Our Inhomogeneous Universe, Phys. Rev. Lett. **125**, 221303 (2020).
[21] A. A. Garcia, K. Bondarenko, S. Ploeckinger, J. Pradler, and A. Sokolenko, Effective photon mass and (dark) photon conversion in the inhomogeneous Universe, J. Cosmol. Astropart. Phys. 10 (2020) 011.
[22] M. Baryakhtar, J. Huang, and R. Lasenby, Axion and hidden photon dark matter detection with multilayer optical haloscopes, Phys. Rev. D **98**, 035006 (2018).
[23] M. Pospelov, A. Ritz, and M. B. Voloshin, Bosonic super-WIMPs as keV-scale dark matter, Phys. Rev. D **78**, 115012 (2008).
[24] H. An, M. Pospelov, J. Pradler, and A. Ritz, Direct detection constraints on dark photon dark matter, Phys. Lett. B **747**, 331 (2015),
[25] I. M. Bloch, R. Essig, K. Tobioka, T. Volansky, and T.-T. Yu, Searching for dark absorption with direct detection experiments, J. High Energy Phys. 06 (2017) 087.
[26] E. Aprile *et al.* (XENON Collaboration), Light Dark Matter Search with Ionization Signals in XENON1T, Phys. Rev. Lett. **123**, 251801 (2019).
[27] H. An, M. Pospelov, and J. Pradler, New stellar constraints on dark photons, Phys. Lett. B **725**, 190 (2013).
[28] J. Redondo and G. Raffelt, Solar constraints on hidden photons re-visited, J. Cosmol. Astropart. Phys. 08 (2013) 034.
[29] N. Vinyoles, A. Serenelli, F. L. Villante, S. Basu, J. Redondo, and J. Isern, New axion and hidden photon constraints from a solar data global fit, J. Cosmol. Astropart. Phys. 10 (2015) 015.
[30] H. An, M. Pospelov, J. Pradler, and A. Ritz, New limits on dark photons from solar emission and keV scale dark matter, Phys. Rev. D **102**, 115022 (2020).
[31] H. An, M. Pospelov, and J. Pradler, Dark Matter Detectors as Dark Photon Helioscopes, Phys. Rev. Lett. **111**, 041302 (2013).
[32] Z. She *et al.* (CDEX Collaboration), Direct Detection Constraints on Dark Photons with the CDEX-10 Experiment at the China Jinping Underground Laboratory, Phys. Rev. Lett. **124**, 111301 (2020).
[33] Y. Ema, K. Nakayama, and Y. Tang, Production of purely gravitational dark matter: The case of fermion and vector boson, J. High Energy Phys. 07 (2019) 060.
[34] R. T. Co, A. Pierce, Z. Zhang, and Y. Zhao, Dark photon dark matter produced by axion oscillations, Phys. Rev. D **99**, 075002 (2019).
[35] J. A. Dror, K. Harigaya, and V. Narayan, Parametric resonance production of ultralight vector dark matter, Phys. Rev. D **99**, 035036 (2019).
[36] M. Bastero-Gil, J. Santiago, L. Ubaldi, and R. Vega-Morales, Vector dark matter production at the end of inflation, J. Cosmol. Astropart. Phys. 04 (2019) 015.
[37] P. Agrawal, N. Kitajima, M. Reece, T. Sekiguchi, and F. Takahashi, Relic abundance of dark photon dark matter, Phys. Lett. B **801**, 135136 (2020).
[38] A. J. Long and L.-T. Wang, Dark photon dark matter from a network of cosmic strings, Phys. Rev. D **99**, 063529 (2019).
[39] G. Alonso-Álvarez, T. Hugle, and J. Jaeckel, Misalignment & Co.: (Pseudo-)scalar and vector dark matter with curvature couplings, J. Cosmol. Astropart. Phys. 02 (2020) 014.
[40] K. Nakayama, Vector coherent oscillation dark matter, J. Cosmol. Astropart. Phys. 10 (2019) 019.
[41] Y. Nakai, R. Namba, and Z. Wang, Light dark photon dark matter from inflation, J. High Energy Phys. 12 (2020) 170.

[42] S. De Panfilis, A. C. Melissinos, B. E. Moskowitz, J. T. Rogers, Y. K. Semertzidis, W. U. Wuensch, H. J. Halama, A. G. Prodell, W. B. Fowler, and F. A. Nezrick, Limits on the Abundance and Coupling of Cosmic Axions at $4.5 < m(a) < 5.0$ μeV, Phys. Rev. Lett. **59**, 839 (1987).
[43] W. U. Wuensch, S. De Panfilis-Wuensch, Y. K. Semertzidis, J. T. Rogers, A. C. Melissinos, H. J. Halama, B. E. Moskowitz, A. G. Prodell, W. B. Fowler, and F. A. Nezrick, Results of a laboratory search for cosmic axions and other weakly coupled light particles, Phys. Rev. D **40**, 3153 (1989).
[44] C. Hagmann, P. Sikivie, N. S. Sullivan, and D. B. Tanner, Results from a search for cosmic axions, Phys. Rev. D **42**, 1297 (1990).
[45] S. J. Asztalos *et al.* (ADMX Collaboration), Large scale microwave cavity search for dark matter axions, Phys. Rev. D **64**, 092003 (2001).
[46] S. J. Asztalos *et al.* (ADMX Collaboration), A SQUID-Based Microwave Cavity Search for Dark-Matter Axions, Phys. Rev. Lett. **104**, 041301 (2010).
[47] L. H. Nguyen, A. Lobanov, and D. Horns, First results from the WISPDMX radio frequency cavity searches for hidden photon dark matter, J. Cosmol. Astropart. Phys. 10 (2019) 014.
[48] D. Horns, J. Jaeckel, A. Lindner, A. Lobanov, J. Redondo, and A. Ringwald, Searching for WISPy cold dark matter with a dish antenna, J. Cosmol. Astropart. Phys. 04 (2013) 016.
[49] S. Knirck, T. Yamazaki, Y. Okesaku, S. Asai, T. Idehara, and T. Inada, First results from a hidden photon dark matter search in the meV sector using a plane-parabolic mirror system, J. Cosmol. Astropart. Phys. 11 (2018) 031.
[50] G. B. Gelmini, A. J. Millar, V. Takhistov, and E. Vitagliano, Probing dark photons with plasma haloscopes, Phys. Rev. D **102**, 043003 (2020).
[51] M. P. van Haarlem *et al.*, LOFAR: The low-frequency array, Astron. Astrophys. **556**, A2 (2013).
[52] S. Collaboration, SKA1 info sheets: The telescopes, 2018, https://www.skatelescope.org/technical/info-sheets/.
[53] V. De La Luz, A. Lara, E. Mendoza, and M. Shimojo, 3D simulations of the quiet sun radio emission at millimeter and submillimeter wavelengths, Geofisica internacional : revista de la Union Geofisica Mexicana auspiciada por el Instituto de Geofisica de la Universidad Nacional Autonoma de Mexico **47**, 197 (2008).
[54] G. Raffelt and L. Stodolsky, Mixing of the photon with low mass particles, Phys. Rev. D **37**, 1237 (1988).
[55] See Supplemental Material at http://link.aps.org/supplemental/10.1103/PhysRevLett.126.181102 for detailed conversion probability calculations, solar model and uncertainty discussions.
[56] J. Redondo, Helioscope bounds on hidden sector photons, J. Cosmol. Astropart. Phys. 07 (2008) 008.
[57] J. E. Vernazza, E. H. Avrett, and R. Loeser, Structure of the solar chromosphere. III. Models of the EUV brightness components of the quiet sun, Astrophys. J. Suppl. Ser. **45**, 635 (1981).
[58] M. J. Aschwanden and L. W. Acton, Temperature tomography of the soft x-ray corona: Measurements of electron densities, temperatures, and differential emission measure distributions above the limb, Astrophys. J. **550**, 475 (2001).
[59] A. H. Gabriel, A magnetic model of the solar transition region, Phil. Trans. R. Soc. A **281**, 339 (1976).
[60] P. Foukal, *Solar Astrophysics* (Wiley, New York, 1990).
[61] M. Aschwanden, *Physics of the Solar Corona: An Introduction with Problems and Solutions*, Springer Praxis Books (Springer, Berlin Heidelberg, 2006).
[62] J. M. Fontenla, E. H. Avrett, and R. Loeser, Energy balance in the solar transition region. I. Hydrostatic thermal models with ambipolar diffusion, Astrophys. J. **355**, 700 (1990).
[63] J. W. Brosius, J. M. Davila, R. J. Thomas, and B. C. Monsignori-Fossi, Measuring active and quiet-sun coronal plasma properties with extreme-ultraviolet spectra from SERTS, Astrophys. J. **106**, 143 (1996).
[64] S. Collaboration, SKA1 system baseline design, Document number: SKA-TEL-SKO-DD-001, 2013, https://www.skatelescope.org/wp-content/uploads/2014/11/SKA-TEL-SKO-0000002-AG-BD-DD-Rev01-SKA1_System_Baseline_Design.pdf.
[65] R. J. Nijboer, M. Pandey-Pommier, and A. G. de Bruyn, LOFAR imaging capabilities and system sensitivity, arXiv:1308.4267.
[66] D. E. Morosan, E. P. Carley, L. A. Hayes, S. A. Murray, P. Zucca, R. A. Fallows, J. McCauley, E. K. J. Kilpua, G. Mann, C. Vocks, and P. T. Gallagher, Multiple regions of shock-accelerated particles during a solar coronal mass ejection, Nat. Astron. **3**, 452 (2019).
[67] C. Ho, A. Kantak, S. Slobin, and D. Morabito, Link analysis of a telecommunications system on earth, in geostationary orbit, and at the moon: Atmospheric attenuation and noise temperature effects, Interplanet. Network Prog. Rep. **42–168**, 1 (2007).
[68] C. Ho, S. Slobin, A. Kantak, and S. Asmar, Solar brightness temperature and corresponding antenna noise temperature at microwave frequencies, Interplanet. Network Prog. Rep. **42–175**, 1 (2008).
[69] D. R. Sinclair, A study of the square kilometre array low-frequency aperture array, Ph.D. thesis, University of Oxford, 2015.
[70] J. D. Kraus, *Radio Astronomy*, 2nd ed. (Cygnus-Quasar Books, Powell, OH, 1986).
[71] J. E. Salah, C. J. Lonsdale, D. Oberoi, R. J. Cappallo, and J. C. Kasper, Space weather capabilities of low frequency radio arrays, in *Solar Physics and Space Weather Instrumentation*, edited by S. Fineschi and R. A. Viereck, Society of Photo-Optical Instrumentation Engineers (SPIE) Conference Series Vol. 5901 (SPIE, Bellingham, 2005), pp. 124–134.
[72] R. Giovanelli *et al.*, The Arecibo Legacy fast ALFA survey. 1. Science goals, survey design and strategy, Astron. J. **130**, 2598 (2005).
[73] The Karl G. Jansky very large array, https://science.nrao.edu/facilities/vla.
[74] R. Nan, D. Li, C. Jin, Q. Wang, L. Zhu, W. Zhu, H. Zhang, Y. Yue, and L. Qian, The five-hundred-meter aperture spherical radio telescope (FAST) project, Int. J. Mod. Phys. D **20**, 989 (2011).